Modeling the fate of organic micropollutant mixture effects in rivers under unsteady flow conditions

Ran Wei,[†] Beate I. Escher,[†,‡] Clarissa Glaser,[†] Maria König,[‡] Rita Schlichting,[‡] Markus Schmitt,[†] Anna Störiko,[†] Michelle Viswanathan,[¶] and Christiane Zarfl[*,†]

[†]*Center for Applied Geoscience, Eberhard Karls University of Tübingen, Tübingen, Germany*

[‡]*Department of Cell Toxicology, UFZ-Helmholtz Centre for Environmental Research, Leipzig, Germany*

[¶]*Institute of Soil Science and Land Evaluation, University of Hohenheim, Hohenheim, Germany*

*Corresponding Author

E-mail: christiane.zarfl@uni-tuebingen.de

Phone: + (49) 7071/29 - 76076. Fax: +(49) 7071 / 29 - 5059

Abstract

The presence of anthropogenic organic micropollutants in rivers poses a long-term threat to surface water quality. To describe and quantify the in-stream fate of single chemicals, the advection-dispersion-reaction (ADR) equation has been used. understanding processes of the cumulative effects caused by micropollutants mixture in rivers requires a new concept. Thus, we extended the ADR from single chemicals to defined mixtures, then to the measured mixture effects of chemicals extracted from the same river water samples, expressed as effect units (EU) and toxic units (TU) (the inverse of effect concentrations and inhibitory concentrations, respectively, quantified with a panel of *in vitro* bioassays). We performed a Lagrangian sampling campaign under unsteady flow, collecting river water containing micropollutants mainly originating from a wastewater treatment plant (WWTP). A convolution-based reactive transport model was used to simulate the dynamics of the effects. For the individual micropollutants' effects, their dissipation dynamics were reproduced by the deterministic model following first-order kinetics. The model ensemble computed within Bayesian inference was needed to characterize the dynamics in the case of experimental mixture effects without known compositions. The highly fluctuating WWTP effluent discharge dominated the temporal patterns of the effect fluxes with minor inputs likely from surface runoff and pesticide diffusion.

Keywords

Bioassay; Effect unit; Cytotoxicity; Markov chain Monte Carlo; Convolution; Reactive transport; Lagrangian sampling.

Synopsis

A stochastic convolution-based reactive transport model effectively characterized the in-stream dynamics of the mixture effect fluxes of micropollutants from diverse sources but

mainly stemming from one wastewater treatment plant.

1 Introduction

Organic micropollutants like pharmaceuticals, polycyclic aromatic hydrocarbons (PAHs), personal care products (PCPs) (e.g., fragrances), detergents, industrial chemicals (e.g., roof sealing) and pesticides have been found ubiquitously at low concentrations levels (in a ng/L-range) in surface waters. The diverse physicochemical properties of these so-called micropollutants can adversely affect their biological and chemical removal efficiencies in the secondary treatment.[1] Even the wastewater treatment plants (WWTPs) equipped with advanced processes have difficulties to completely eliminate all the micropollutants.[2–4] WWTPs have been viewed as one of the main sources of organic micropollutants in rivers.[5,6] Especially in small rivers where the surrounding areas are densely populated and the river discharge is dominated by the WWTP's effluent, the receiving river water quality may be adversely impacted by WWTPs effluent.[7–10]

To understand the micropollutant dynamics and their potential risk, some previous studies applied the Lagrangian sampling scheme with high temporal resolutions to collect composite samples in rivers. The scheme captures the in-stream dynamics of the micropollutants by tracking the same water packages from upstream to downstream locations.[11–13] These studies were purely focusing on the concentrations of the micropollutants, inorganic ions and dissolved organic carbon (DOC). Numerous studies have also been conducted on individual and mixture effects (specific effects and cytotoxicity) from WWTPs-emitted micropollutant mixtures[14,15] in rivers. The main aims of these studies were to identify the micropollutants in the complex mixtures and the individual contributions to the overall mixture effects. It is not possible to identify every single compound in the complex mixture that potentially consists of hundreds and thousands of chemicals. But the effects stemming from the individual compounds, as well as the ones characterizing the overall mixture effects, can be quantified

in the panels of *in vitro* bioassays. When thousands of compounds are present at very low concentrations in mixtures, the interactions among them are usually not noticeable. Under such circumstances, the concentration addition concept can be applied.[16]

The fast changing in-stream dynamics of individual and mixture effects have been studied by Müller et al..[10,17] However, there is a lack of quantitative understanding of the in-stream processes that the mixture effects undergo. Uncertainties originating from the quantification of the total bioactive mixture effects also need to be taken into account when studying the fate of mixture effects. A process-based mathematical modeling approach is needed to gain quantitative insights of in-stream mechanisms of the mixture effects. Liu et al.[18] studied the in-stream fate of a few pharmaceuticals using a one-dimensional reactive transport model. The computation expense of the model is already relatively high due to the complex parameterization and spatial discretization. To address uncertainties that lead to the unclear transport pattern in the mixture effects data to reflect the random nature of the system and displaying levels of belief in the modeled results (as well as the model structure), a time series ensemble is particularly useful. Coupled with stochastic methods, the measurement uncertainties are taken into account when approximating the model parameters' distributions, from where ensemble results can be computed. Thus, the computation costs increase with the complexity of the micropollutant mixtures that contain a large number of compounds, of which the individual and total mixture effects are quantified in multiple bioassays. The simulation time can be the limiting factor to run the model if stochastic methods are to be applied, when hundreds of thousands of model runs are needed for each mixture effect simulation.

The present study intended to evaluate if a one-dimensional model based on the advection-dispersion-reaction equation (ADR) is able to characterize the in-stream dynamics of specific effects and of the cytotoxicity of both individual compounds and the total bioactive micropollutant mixture. We assumed that parameters for the transport and reactions that characterize the single chemical's fate can be transferred to the dynamics of the mixture

effects in rivers. We tested our hypothesis by combining a Lagrangian sampling campaign in a WWTP influenced river with the measurement of chemical mixtures and their effects. We implemented a computationally cheap convolution-based transport model to simulate the unsteady discharge in the river main channel caused by the WWTP high release. Adding first-order reaction kinetics, the convolution-based reactive transport model was applied to the individual compounds effects. The mixture effects of all chemicals in water samples were modeled by coupling the deterministic model with Metropolis-Hastings Markov chain Monte Carlo (MH-MCMC) to account for measurement and parameter uncertainties and which overcame the less clear transport patterns in the observations.

2 Theory

Effect unit and toxic unit. The specific effects (e.g. estrogenic effects, triggered by binding of micropollutants and natural hormones to the estrogen receptor.[19]) and cytotoxicity in the river water, stemming from the micropollutants contributed mainly by WWTPs, were quantified in *in vitro* bioassays and expressed as effect unit (EU) for specific effects and toxic unit (TU) for cytotoxicity. Both EU and TU can be used to characterize the effects of individual chemicals ($EU_{\mathrm{chem}_i,\mathrm{assay}_j}$, Eq. 1 and $TU_{\mathrm{chem}_i,\mathrm{assay}_j}$, Eq. 2), the mixture effects of the detected chemicals in the sample ($EU_{\mathrm{chem},\mathrm{assay}_j}$ and $TU_{\mathrm{chem},\mathrm{assay}_j}$), as well as the experimentally quantified mixture effects (EU_{bio} and TU_{bio}).

$$EU_{\mathrm{chem}_i,\mathrm{assay}_j} = \frac{C_{\mathrm{chem}_i}}{EC_{k,\mathrm{chem}_i,\mathrm{assay}_j}} \tag{1}$$

$$TU_{\mathrm{chem}_i,\mathrm{assay}_j} = \frac{C_{\mathrm{chem}_i}}{IC_{k,\mathrm{chem}_i,\mathrm{assay}_j,\mathrm{exp}}} \tag{2}$$

C_{chem_i} [ng L^{-1}] is the concentration of the individual detected compound. EC_{k,chem_i} [ng L^{-1}] and IC_{k,chem_i} [ng L^{-1}] are the compound specific effect concentration (EC) and inhibition

concentration (IC) that causes k effects (k typically is 10 % of the maximum effect[20] or the induction ratio (IR) of 1.5, which is 50% over unexposed cells of IR 1.[17,20]) of specific endpoints and cell death (cytotoxicity), respectively. i and j are individual compounds' and bioassays' indices, respectively. n is the number of the compounds detected in the water sample and activated in the corresponding assay j.

The mixture effects of all detected and activated compounds, $EU_{\mathrm{chem,assay}_j}$ (Eq. 3) and $TU_{\mathrm{chem,assay}_j}$ (Eq. 4), are the sum of the individual compounds' effects.

$$EU_{\mathrm{chem,assay}_j} = \sum_{i=1}^{n} \frac{C_{\mathrm{chem}_i}}{EC_{k,\mathrm{chem}_i,\mathrm{assay}_j}} \tag{3}$$

$$TU_{\mathrm{chem,assay}_j} = \sum_{i=1}^{n} \frac{C_{\mathrm{chem}_i}}{IC_{k,\mathrm{chem}_i,\mathrm{assay}_j,\mathrm{exp}}} \tag{4}$$

The EU and TU describing the mixture effects of the whole water sample, EU_{bio_j} [$\mathrm{L_{biosassy}} \cdot \mathrm{L_{water}}^{-1}$] (Eq. 5) and TU_{bio_j} [$\mathrm{L_{biosassy}} \cdot \mathrm{L_{water}}^{-1}$] (Eq. 6).

$$EU_{\mathrm{bio}_j} = \frac{1}{EC_{k,\mathrm{assay}_j}} \tag{5}$$

$$TU_{\mathrm{bio}_j} = \frac{1}{IC_{k,\mathrm{assay}_j}} \tag{6}$$

where EC_{k,assay_j} and IC_{k,assay_j} are the ECs and ICs of the whole water sample that trigger k effects and cytotoxicity, respectively. The units of EC and IC are relative enrichment factor (REF).[19] For TU of the whole bioactive mixture (TU_{bio}), the measured TU_{bio} values in different bioassays should be relatively similar, since TUs are quantified based on the same endpoint. The mean TU_{bio} of four bioassays (bioassay details in Section 3.2) were used in this study.

Effect unit and toxic unit fluxes. The fluxes $F_k(t)$ of the EU ($q = EU_{\text{chem}i,\,\text{assay}_j}$, EU_{bio_j}) and the TU ($q = TU_{\text{chem}i,\,\text{assay}_j}$, TU_{bio_j}) are defined by the products of the effect units and toxic units, respectively, with the corresponding discharge (Q in [m^3 s^{-1}]) at time t (Eq. 7. EU is replaced by TU when computing the cytotoxicity flux).

$$F_q(t) = EU_q(t) \cdot Q(t) \tag{7}$$

Conservative transport of electrical conductivity. The electrical conductivity (ECd) in rivers is assumed to behave identically to the conservative compounds or ideal tracer.[11,12] Therefore, the ECd time series can be used to determine the hydrological parameters values, e.g., the mean water travel time and the lumped advection and dispersion coefficient[11,12,21] by fitting the modeled ECd to the measurements (fitting details in Section 3.3). In general, the one-dimensional transport of a time series signal in rivers can be described by a linear time-invariant system and its impulse response in the time domain. The essence is that the output signal is the integral of the product of the input signal and a transfer function. This operation is named convolution and can be expressed for the ECd by Eq. 8,

$$ECd_{\text{down}}(t) = \int_0^t ECd_{\text{up}}(t-\tau)g(\tau)d\tau \tag{8}$$

where ECd_{up} [mS cm^{-1}] and ECd_{down} [mS cm^{-1}] are the ECd time series at the upstream and the downstream locations of the studied river stretch, respectively. t is the sampling time point. τ is the travel time of the individual water parcel, and $g(\tau)$ is the transfer function.

Conservative transfer function. The impulse response of a linear-time invariant system is the transfer function, which is a probability density function (PDF) that characterizes the distribution of the travel times (τ) of the water parcels and produces the downstream signal from the upstream signal via convolution. Assuming ECd behaves conservatively, the transfer

function consists of advection and dispersion terms,[11,12,22] and is expressed as Eq. 9,

$$g(\tau) = \frac{1}{\tau\sqrt{\frac{4\pi D\tau}{\Delta t_{\mathrm{ECd}}}}} \exp\left(-\frac{(1-\frac{\tau}{\Delta t_{\mathrm{ECd}}})^2}{\frac{4D\tau}{\Delta t_{\mathrm{ECd}}}}\right) \tag{9}$$

which is parameterized by the dimensionless dispersion coefficient D [-] and the mean travel time Δt_{ECd}.

Unsteady discharge propagation. For approximating downstream discharge (Q_{down}) under unsteady flow conditions, an earlier approach for steady state conditions by Schwientek et al.[11] was adopted in Eq. 10,

$$Q_{\mathrm{down}}(t) = \int_0^t Q_{\mathrm{up}}(t-\tau)q(\tau)d\tau \tag{10}$$

where $Q_{\mathrm{down}}(t)$ [volume time^{-1}] and $Q_{\mathrm{up}}(t)$ [volume time^{-1}] are the discharge time series at the upstream and downstream locations, respectively (Q_{up} calculation in Text S1). The mean travel time of the wave is different from that of the ECd, therefore, the transfer function $q(\tau)$ needs to be adjusted as Eq. 11.

$$q(\tau) = \frac{1}{\tau\sqrt{\frac{20\pi D\tau}{3\Delta t_{\mathrm{ECd}}}}} \exp\left(-\frac{(1-\frac{5\tau}{3\Delta t_{\mathrm{ECd}}})^2}{\frac{20D\tau}{3\Delta t_{\mathrm{ECd}}}}\right) \tag{11}$$

The unsteady discharge follows the travel phenomenon of the kinematic wave in the open channel. Since the studied river stretch forms a rectangular channel and the water depth is shallow relative to the channel width, the definition of the celerity $c_{\mathrm{kn,wave}}$ [m s^{-1}] of the wave in relation to the mean velocity of the ECd v_{ECd} [m s^{-1}], can be simplified to Eq. 12,[11,23]

$$c_{\mathrm{kn,wave}} = \frac{5}{3}v_{\mathrm{ECd}} \tag{12}$$

which gives to Eq. 13,

$$\Delta t_{\mathrm{kn,wave}} = \frac{3}{5}\Delta t_{\mathrm{ECd}} \tag{13}$$

where $\Delta t_{\mathrm{kn,wave}}$ is the mean kinematic wave travel time.

Reactive transport of the effects from individual chemicals and mixture. In addition to the transport processes described above for the EU and TU, these effects are undergo exponential first-order decay. Therefore, the transport of the EU and TU is complemented by a description of the lumped loss process following first-order kinetics (Eq. 14 – 17),

$$EU_{\mathrm{chem}_i,\mathrm{assay}_j,\mathrm{down}}(t) = \int_0^t EU_{\mathrm{chem}_i,\mathrm{assay}_j,\mathrm{up}}(t-\tau) r_{\mathrm{chem}_i}(\tau) d\tau \tag{14}$$

$$TU_{\mathrm{chem}_i,\mathrm{assay}_j,\mathrm{down}}(t) = \int_0^t TU_{\mathrm{chem}_i,\mathrm{assay}_j,\mathrm{up}}(t-\tau) r_{\mathrm{chem}_i}(\tau) d\tau \tag{15}$$

$$EU_{\mathrm{bio}_j,\mathrm{down}}(t) = \int_0^t EU_{\mathrm{bio}_j,\mathrm{up}}(t-\tau) r_{\mathrm{bio}_j,\mathrm{spec}}(\tau) d\tau \tag{16}$$

$$TU_{\mathrm{bio}_j,\mathrm{down}}(t) = \int_0^t TU_{\mathrm{bio}_j,\mathrm{up}}(t-\tau) r_{\mathrm{bio}_j,\mathrm{cyto}}(\tau) d\tau \tag{17}$$

where the $EU_{\mathrm{chem}_i,\mathrm{assay}_j}$, $TU_{\mathrm{chem}_i,\mathrm{assay}_j}$, EU_{bio_j} and TU_{bio_j} are time series of the state variables defined in Eq. 1 – 6. $r_{\mathrm{chem}_i}(\tau)$, $r_{\mathrm{bio}_j,\mathrm{spec}}(\tau)$ and $r_{\mathrm{bio}_j,\mathrm{cyto}}(\tau)$ are compound and assay specific reactive transfer functions, respectively that relate to the conservative transfer function $g(\tau)$ (Eq. 9) by Eq. 18 – 20.

$$r_{\mathrm{chem}_i}(\tau) = g(\tau)\exp(-\lambda_{\mathrm{chem}_i}\tau) \tag{18}$$

$$r_{\mathrm{bio}_j,\mathrm{spec}}(\tau) = g(\tau)\exp(-\lambda_{\mathrm{bio}_j,\mathrm{spec}}\tau) \tag{19}$$

$$r_{\mathrm{bio}_j,\mathrm{cyto}}(\tau) = g(\tau)\exp(-\lambda_{\mathrm{bio}_j,\mathrm{cyto}}\tau) \tag{20}$$

where $\lambda_{\mathrm{chem}_i}$, $\lambda_{\mathrm{bio}_j,\mathrm{spec}}$ and $\lambda_{\mathrm{bio}_j,\mathrm{cyto}}$ are the compound-specific and assay-specific reaction rate constants [time^{-1}] that are, in this case, assumed to be constant over time. The transient storage part (needed under low flow conditions[18]) of the model was ignored in this case.

3 Materials and Methods

General approach. We conducted model-aided scenario analysis (Text S2) prior to the sampling and applied a Lagrangian sampling scheme that follows the same water parcel along the course of the Steinlach River in Tübingen (southwestern Germany). The studied river stretch is under direct impacts from a wastewater treatment plant effluent. Three auto-samplers have been installed for 46 hours to collect composite time series water samples. Samples from the field have been analyzed on concentrations and effects. A one-dimensional reactive convolution model coupled with stochastic methods has been developed for describing the fate of the effects along the river.

3.1 Field campaign

The underlying sampling campaign took place in summer (June to August) 2020 at the Steinlach River with a mean discharge of 1.83 m^3s^{-1} and a WWTP effluent of 0.26 m^3s^{-1} close to the city of Tübingen, Germany. More details on field site and the sampling campaign can be found in the Supporting Information (Text S3).

Mean travel time. Prior to the sampling, it was crucial to estimate the mean water parcel travel time so that the starting time of the auto-samplers at different sampling sites could be determined. We assumed that 1) the ECd signal behaves conservatively, 2) it reflects the temporal variation resulting from the effluent flow of the WWTP and 3) the measured

ECd values as a result of the existing organic substances in the water are much higher than the background ECd values in the main channel. The mean travel time estimation method presented by Schwientek et al.[11] and Glaser et al.[12] was modified by implementing the MultiStart algorithm to find the global solution in this study. We fitted the modeled downstream ECd to the measured ECd, deriving the transfer function's parameters, the mean travel time Δt_{ECd} and the lumped apparent dispersion coefficient D (Section 3.3). ECd measurement prior the sampling and correcting scheme are in Text S4 in Figure S2 - Figure S5.

3.2 Laboratory work

A brief description of the chemical analysis of the micropollutants (previously published[24]) can be found in the Supporting Information (Text S5).

***In vitro* bioassays.** The whole water samples were tested on four *in vitro* bioassays named AhR-CALUX (AhR) for aryl hydrocarbon receptor induction, PPARγ-GeneBLAzer (PPARγ) for peroxisome proliferator-activated receptor activity, ERα-GeneBLAzer (ER) for estrogenicity and AREc32 (ARE) for oxidative stress. Examples of inducing compounds for the four bioassays are polycyclic aromatic hydrocarbons (PAHs), fibrate pharmaceuticals, endocrine-disrupting compounds and pharmaceuticals that could produce reactive oxygen species, respectively.[19] In each cell line, the cytotoxicity was also measured. The effect concentration and inhibitory concentration (EC_{10} and IC_{10}) that cause 10% of the effects were quantified by fitting a simple linear regression in the concentration-response curve.[25] Detailed information on the measuring methods can be found in König et al..[26]

3.3 Parameter estimation: Deterministic method

The nonlinear least-squares solver was used in estimating the mean travel time Δt_{ECd}, the lumped dispersion coefficient D (Eq. 9), and the first-order reaction rate constant of the

detected individual compound's effect (Eq. 18). The objective function was defined as:

$$\min_{\theta}(f(\theta)) = \sum_{i=1}^{n}(f(\theta, xdata_i) - ydata_i)^2 \tag{21}$$

where θ is the parameter to be found given the input ($xdata$) and observation ($ydata$). The MultiStart algorithm (trust-region-reflective searching method) was used to evaluate the outcome of the objective function. The global solution was found from the results of local solvers with multiple (500 - 1500) starting points. Normalized root-mean-square error (NRMSE) was computed for each compound to evaluate the goodness of the model fit. NRMSE is defined as the root mean square error divided by the difference between the maximum ($ydata_{\text{obs,max}}$) and minimum values ($ydata_{\text{obs,min}}$) in the observations (Eq. 22).

$$\text{NRMSE} = \frac{\sqrt{\sum_{i=1}^{n}(ydata_{\text{model},i} - ydata_{\text{obs},i})^2/n}}{ydata_{\text{obs,max}} - ydata_{\text{obs,min}}} \tag{22}$$

3.4 Parameters estimation: Markov chain Monte Carlo

The Metropolis–Hastings Markov chain Monte Carlo (MH-MCMC) algorithm was applied in modeling the total effect and toxic units, EU_{bio} and TU_{bio} (Eq. 5 – 6).

The prior parameter distribution. A prior distribution represents the belief of the existing information, knowledge or assumptions (e.g., parameters values and their uncertainty), before any observations are provided.[27] The form and bounds of a prior distribution of the parameter(s) to be estimated can be derived based on existing theories, hypothesis, past experiments or simply experience and constrains due to logical reasons. According to Gelman et al.,[28] in theory the range of the prior distribution should be wide enough to cover all possible parameters' values. Therefore, we firstly assumed that the prior distribution of the first-order reaction constants of EU_{bio_j} is informative and normal. A normal distribution was fitted to the deterministically calibrated first-order reaction constants of all the detected organic micropollutants (Section 3.3), and their correspond-

ing reaction rate constants derived from the literature half-lives (Predicted biodegradation half-life values from quantitative structure–activity/property relationship (QSAR) model.[29] `https://comptox.epa.gov/dashboard`) using Eq. 23,

$$\lambda_i = \frac{\ln(2)}{t_{1/2,i}} \tag{23}$$

where $t_{1/2}$ [time] is the literature half-life value, λ [time^{-1}] the first-order reaction constant, and i [-] the compound's index. The parameters of the normal distribution $\boldsymbol{\lambda} \sim \mathcal{N}(\mu, \sigma^2)$ thus can be determined and the log PDF is

$$LnPrior(\lambda) = \ln\left[\frac{1}{\sigma_\lambda\sqrt{2\pi}} e^{-\frac{1}{2}\left(\frac{\lambda-\mu_\lambda}{\sigma_\lambda}\right)^2}\right] \tag{24}$$

The standard deviation σ_ϵ in the likelihood function (Eq. 26 below) was treated as a variable also sampled by MH-MCMC. The prior distribution of σ_ϵ was assumed to be a bounded uniform distribution, of which the lower boundary is zero. σ_ϵ represents the measurement error of the data, however this information can not be used to construct the prior distribution if it comes from the observations that are used during the posterior sampling process. The maximum value ($\sigma_{\epsilon,\max}$) from the reported standard errors of the measured values of the grab samples collected at the WWTP effluent and 20% of the measurements' values[19] was computed. In an effort to cover as many reasonable values as possible, the upper boundary of the uniform distribution was set to be five times of the $\sigma_{\epsilon,\max}$ ($\sigma_\epsilon \sim \mathcal{U}(0, ub)$ and $ub = 5\sigma_{\epsilon,\max}$). The log PDF is expressed as

$$LnPrior(\sigma) = \ln(\frac{1}{ub}) \tag{25}$$

Therefore, the hyperparameters (parameters of the prior distribution) are defined and the log probability density can be computed.

The likelihood function. The model errors were assumed to be identically and independently distributed (IID). Apart from the first-order reaction rate constant λ, the standard

deviation σ_ϵ in the likelihood function is also a variable that is sampled by MH-MCMC. If $\mathbf{\Theta} = [\lambda, \sigma_\epsilon]^T$ is the parameter vector, $\mathbf{y}_{\text{obs}} = [y_{\text{obs},1}, ..., y_{\text{obs},n}]$ the observation vector, then the log-likelihood function is defined as

$$LL(\mathbf{\Theta}|\mathbf{y}_{\text{obs}}) = \sum_{i=1}^{n} \ln\left(\frac{1}{\sqrt{2\pi\sigma_{\epsilon,i}}} \exp\left[-\frac{1}{2}\frac{(y_{\text{model},i}(\lambda_i) - y_{\text{obs},i})^2}{\sigma_{\epsilon,i}^2}\right]\right) \tag{26}$$

where i [-] is the observation index, n [-] the total number of the observations. Thus, by rearranging Eq. 24 – 26, the log posterior distribution is expressed as

$$\begin{aligned} LnPost(\mathbf{\Theta}|\mathbf{y}_{\text{obs}}) = \ln \prod_{i=1}^{n} \Bigg(&\frac{1}{\sqrt{2\pi\sigma_{\epsilon,i}}} \exp\left[-\frac{1}{2}\frac{(y_{\text{model},i}(\lambda_i) - y_{\text{obs},i})^2}{\sigma_{\epsilon,i}^2}\right]\Bigg) \\ &\left(\frac{1}{\sigma_\lambda\sqrt{2\pi}} \exp\left[-\frac{1}{2}\left(\frac{\lambda_i - \mu_\lambda}{\sigma_\lambda}\right]\right)^2\right)\frac{1}{ub} \end{aligned} \tag{27}$$

The MH-MCMC algorithm was applied to observations from four cell lines: AhR, PPARγ, ER and AREc32. Five Markov chains ran sequentially. For the five chains to converge, iteration lengths differ (10000 to 50000 iterations each chain), depending on uncertainties in the data from different cell lines. After the burn-in period (the first 50% iterations), chains' convergence was checked using the Gelman-Rubin diagnostic with the potential scale reduction factor $\hat{R} < 1.1$.[30,31]

The starting point of the individual chain is a randomized value (details of randomization in Text S9).

4 Results and Discussion

4.1 ECd signals and unsteady flow

The measured ECd signals at all MS (sampling map: Figure S1) not only characterized the one dimensional in-stream transport phenomenon, but also conveyed information regarding

the background river water quality, exhibiting a clear temporal pattern contrast between upstream and downstream locations from the WWTP effluent. There were no rain events recorded between 20:00, August 19 (AS1 started sampling) and 17:15, August 21 (AS3 stopped sampling), apart from the two low precipitations of 0.22 mm h^{-1} and 0.1 mm h^{-1} at 21:00, August 19 and 06:00, August 20, respectively (`https://www.wetter-bw.de/Internet/AM/NotesBwAM.nsf/bwweb/4262596897754529c1257ca8002f9d19?OpenDocument&TableRow=3.7#3`). During this period, the mean effluent discharge from the WWTP (0.12 m^3 s^{-1}, ± 0.27 m^3 s^{-1}) contributed 47% of the mean discharge in the main channel (0.26 m^3 s^{-1}, ± 0.13 m^3 s^{-1}). A distinct ambient in-stream ECd diurnal cycle was observed at the measuring station upstream (MS Up) from the WWTP, where the dynamics of ECd corresponded to the water temperature temporal pattern (Figure S6). The ECd values at the MS in the main channel downstream from the WWTP were approximately 1.5 times higher than that at MS Up during the sampling period, demonstrating the contribution from the WWTP release. The calibrated hydrological transport parameters based on the ECd time series were used in the unsteady discharge calculation (Figure S7; normalized rooted mean square error (NRMSE) of 0.0093 and 0.0084 (Table S7) for calibration results at MS2 and MS3 respectively). Figure 1 illustrates the modeled discharge in the studied river stretch. The WWTP effluent discharge was relatively steady after AS1 started sampling, but its contribution to the main river flow was high and dynamic. The WWTP effluent prompted the formation of a discharge wave (increase from 0.12 m^3 s^{-1} to the peak of 0.64 m^3 s^{-1} in Figure 1B) that traveled downstream in the main channel, causing flow in the main channel to become unsteady (Figure 1C – E). Overlays of discharge at all MSs demonstrate how the wave propagated (Figure S8). Dissolved organic carbon (DOC) (Figure S9A) was higher at day than at night and was also mainly influenced by the DOC of the WWTP. The pH followed the discharge and was at pH 8 at lower discharged but rose to over 9 at higher discharge (Figure S9B).

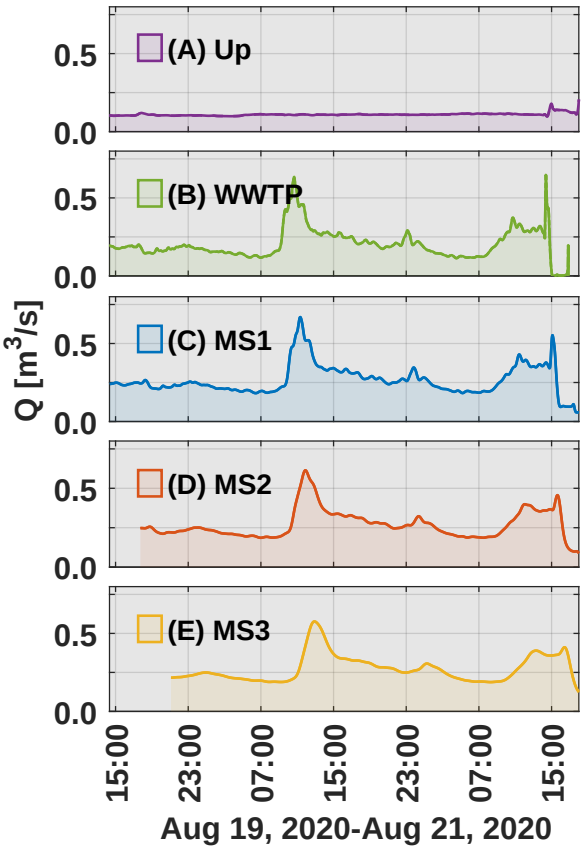

Figure 1: Computed unsteady flow during the sampling period: (A) Discharge at the location upstream from the wastewater treatment plant (Up); (B) Discharge at the wastewater treatment plant effluent (WWTP); (C) Discharge at measuring station one (MS1); (D) Discharge at measuring station two (MS2); (E) Discharge at measuring station three (MS3). Detailed sampling location information can be found in Figure S1.

4.2 In-stream concentration and effect dynamics

Detected chemicals' concentrations and mass fluxes. The in-stream dynamics of the concentrations of the detected micropollutants[14] were captured well by the Lagrangian sampling scheme (Figure S10 – Figure S19, Table S4). The modeled (model details in Eq. S8 – S13) detected compounds' concentrations, as well as their mass fluxes (Figure S20 – Figure S29) matched the observations well (NRMSE in Table S7). All analytical uncertainties were significantly smaller than the temporal variations observed in the data. Therefore, it can be concluded that the observed temporal variations reflected actual in-stream dynamics, not noise from measurement uncertainties.

Individual bioactive chemicals' effects over time and space ($EU_{\mathbf{chem},i}$ and $TU_{\mathbf{chem},i}$). The dynamics of the detected micropollutants' specific effects expressed as $EU_{\mathrm{chem},i}$ and cytotoxicity, $TU_{\mathrm{chem},i}$, are closely related to their concentrations[14] (Eq. 1 – 2). Figure S30 illustrates the measured $EU_{\mathrm{chem},i}$ time series of compounds from MS2 and MS3 that were activating the AhR in AhR-CALUX assay. The pronounced $EU_{\mathrm{chem},i}$ peaks recorded between 12:20 and 14:20 on August 20 were evidently caused by the earlier high release from the WWTP. Furthermore, the simulated time courses of $EU_{\mathrm{chem},i}$ were able to reproduce the temporal variations of the measurements (e.g. the $EU_{\mathrm{chem},i}$ peak for all compounds except 2-Aminobenzothiazole and benzothiazole-2-sulfonic acid), as well as fall within the range of measurements uncertainties. Particularly in the cases of benzotriazole (Figure 2A), diuron and telmisartan (Figure S30), the modeled $EU_{\mathrm{chem},i}$ time courses were able to accurately capture the observed peaks, as well as the tailings (from 21:00 on August 20 to 10:00 on August 21) of the EU dynamics at both MS2 and MS3 (NRMSE (Eq. 22) of the nine compounds in Table S7). Benzothiazole-2-sulfonic acid (B-2-SA) displayed an entirely different temporal pattern from the rest of the eight compounds (Figure 2B). Instead of being elevated by the WWTP input, the $EU_{\mathrm{chem},i}$ observations experienced a drop between 12:20 and 14:20, as well as observable fluctuations between 13:00 and 17:00 at both MSs on August 20. Afterwards, the pronounced peaks were observed at later hours between 21:00 on August 20 and 05:00 on August 21. Previous study[32] found that B-2-SA was the dominant compound among other benzothiazoles in the municipal wastewater and that surface runoff caused a substantial amount of B-2-SA into receiving waters. This conclusion might shed lights on the reason of different temporal pattern found in B-2-SA in our study. Still, the model was capable of reproducing most of the features in B-2-SA data. The modeled $EU_{\mathrm{chem},i}$ time courses for individual compounds in PPARγ and AREc32 can be found in Figure S31 – Figure S32. NRMSE for all detected compounds at MS2 and MS3 are shown in Table S7.

Individual bioactive chemicals' effect unit fluxes. The high release from the WWTP not only functioned as a major contributor of effects in the Steinlach River, but also played a crucial role in characterizing the in-stream temporal patterns of $EU_{\mathrm{chem},i}$ fluxes. The $EU_{\mathrm{chem},i}$ fluxes of B-2-SA and benzotriazole in AhR are shown in Figure 2C – D. The modeled

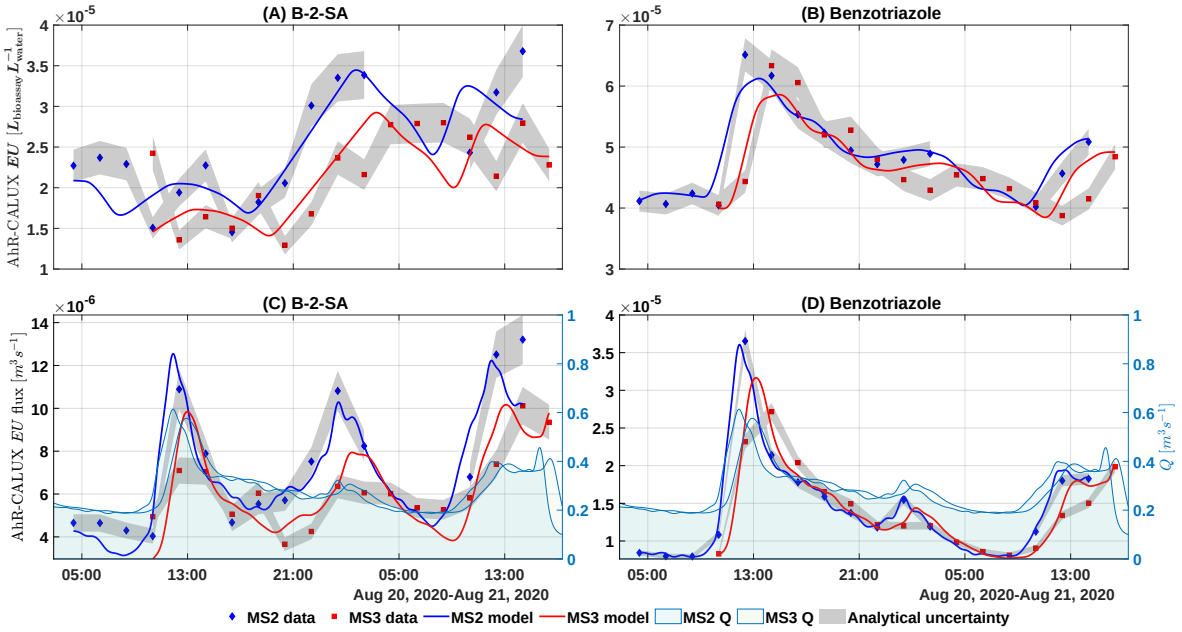

Figure 2: $EU_{\mathrm{chem},i}$ (A) – (B) and $EU_{\mathrm{chem},i}$ fluxes (C) – (D) of the two detected chemicals that were activated in AhR-CALUX. Analytical uncertainties (one standard deviation) originating from the concentration measurements were illustrated in grey area. Discharges at the corresponding locations are shown in light blue and green areas. Abbreviations: B-2-SA – Benzothiazole-2-sulfonic acid; MS – Measuring station.

discharge time series was plotted alongside the $EU_{\mathrm{chem},i}$ fluxes. The major temporal patterns of the $EU_{\mathrm{chem},i}$ for AhR (Figure S30) were masked by the discharge features. The $EU_{\mathrm{chem},i}$ fluxes were heavily shaped by the unsteady discharge. The discharge waves that were caused by the sudden WWTP release led to the $EU_{\mathrm{chem},i}$ fluxes peaked at 12:00 at MS2 and 13:10 at MS3. The modeled $EU_{\mathrm{chem},i}$ fluxes' were able to produce the peaks that propagated from MS2 to MS3 in the observations of 4&5 methyl-benzotriazole, benzotriazole, climbazole, diuron, isoproturon and telmisartan (although slight deviations from the data can been seen, e.g. in the last six hours of sampling period for tramadol.). The $EU_{\mathrm{chem},i}$ flux of B-2-SA, similar to its $EU_{\mathrm{chem},i}$, exhibited a different temporal pattern from the rest of the compounds

that were activating the AhR at both MSs. In particular, the $EU_{\text{chem},i}$ flux of B-2-SA clearly peaked twice during our sampling period, and the modeled results at MS3 showed the largest deviation from the data in comparison to all other compounds approximately at mid-night of August 21st. Nevertheless, the modeled $EU_{\text{chem},i}$ fluxes were able to reproduced the key features in the observations for the detected compounds in AhR-CALUX, PPARγ and AREc32 (Figure S33 - Figure S35).

The model also performed well when applied to the cytotoxicity data. As the $EU_{\text{chem},i}$ and $TU_{\text{chem},i}$ only differed by a scaling factor, the modeled time course of the $TU_{\text{chem},i}$ in six cell lines (AhR, PPARγ, ERα, AREc32, AR-GeneBLAzer (AR) and GR-GeneBLAzer (GR) in Figure S36 – Figure S41) again were able to reproduce the main features of the individual compound's cytotoxicity time series. Similar results can be seen in the case of cytotoxicity fluxes (Figure S42 – Figure S47, Table S7). By applying the convolution-based transport model with the first-order reaction kinetics to the individual effects data, we demonstrated that the model was able to quantitatively characterize in-stream mechanisms of the individual effects.

Predicted mixture effects of bioactive chemicals (EU_{chem} and TU_{chem}). The bioactive detected chemicals are expected to contribute to the mixture effects that were measured in a water sample. Figure 3A – C display the percentages of the mean $EU_{\text{chem},i}$ of the individual micropollutants from MS1 over the whole sampling period. Within the mixture effect EU_{chem} (Eq. 3), the contributions from the individual compounds varied over different bioassays, but did not differ significantly between sampling locations. Benzothiazole-2-sulfonic acid contributed a relatively large fraction of EU_{chem} in AhR, PPARγ and AREc32 (full results can be found in Figure S48 – Figure S49.). In all three bioassays, the contribution of all detected and activated compounds (EU_{chem}) to the total effect (EU_{bio}) was less than 1% regardless of the locations (Figure 3B and D), indicating that the majority of the effects in EU_{bio} were contributed by the non-detected compounds. Neale et al.[33] reported similar low

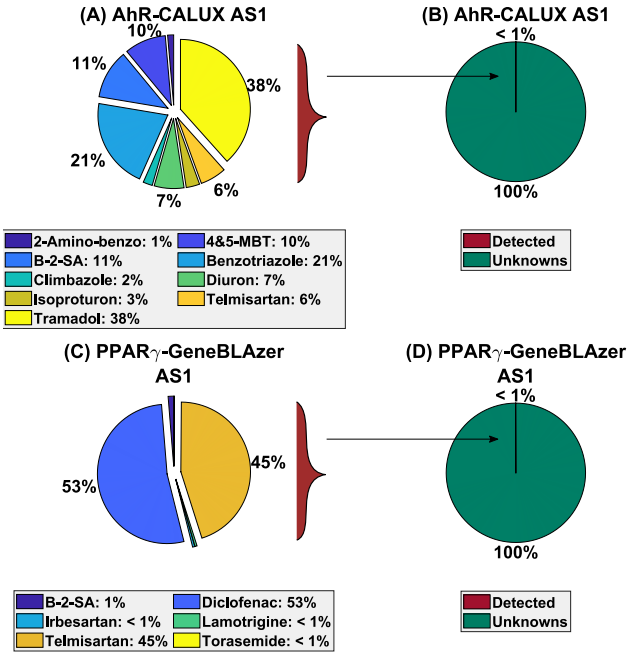

Figure 3: Contribution (%) of the mean effect units over the sampling period from individual micropollutants to the whole mixture at auto-sampler 1 for the bioassay AhR and PPARγ. (A) and (C): Contribution of individual micropollutants effects to EU_{chem}; (B) and (D): Contribution of all detected micropollutants to EU_{bio}; Abbreviations: 2-Amino-benzo – 2-Aminobenzothiazole; 4&5-MBT – 4&5 Methyl-benzotriazole; B-2-SA – Benzothiazole-2-sulfonic acid; Detected – Effect of all detected compounds; Unknowns – Effect of the non-detected compounds. Unit of EU: [$L_{\text{biosassy}} \cdot L_{\text{water}}^{-1}$]

fractions of explained effects in the same three bioassays in water samples from diverse rain events in rivers of similar sizes.

In the case of cytotoxicity, no single compounds showed the universal dominance at contributing individual effects ($TU_{\text{chem},i}$) to the mixture effects of the detected compounds (TU_{chem}) across all bioassays. The percentages of TU contributed by individual compounds to TU_{chem} in AhR, PPARγ, ERα, AREc32, AR and GR are shown in Figure S50 – Figure S52. Diclofenac, benzotriazole, sulpiride and terbutryn contributed the overall high percentages in PPARγ, AR, GR and ERα, respectively. In AhR and AREc32, TU_{chem} was more evenly composed out of the effects of individual compounds. No significant spatial variations of the individual TU contributions were observed.

The time patterns of the mixture effects from all the detected and active compounds, EU_{chem} and TU_{chem} (Eq. 3 – 4), were dominated by those compounds that contributed some

of the largest shares of the effects in the mixture (Figure S53 – Figure S56). Similar to the individual effects, the dynamics of the fluxes were dominated by that of the discharge. Modeled flux results were able to reproduce the major features (e.g. the main peak caused by the WWTP's effluent sudden release) observed in the data from all three bioassays.

The total mixture effects ($EU_{\mathbf{bio}}$ and $TU_{\mathbf{bio}}$) and fluxes. The measured time series and modeled time series ensemble of EU_{bio} in AhR, PPARγ, ERα and AREc32 at MS2 and MS3 are shown in Figure S57 – Figure S58, respectively. The EU_{bio}, representing the total specific burden that resulted from all of the organic micropollutants in the water sample, displayed low variations and unclear transport patterns along the river course (Figure 4) presumably because the discharge was not stable during the sampling period (Figure 1) and therefore the composition of the components triggering the mixture effect were highly variable. Similar to the $EU_{\text{chem},i}$ fluxes of the detected compounds, as well as the results from Müller et al.[34] in storm events, in this study the observed fluxes of EU_{bio} were mainly dominated by the temporal patterns of the unsteady discharge (Figure 4). In all four bioassays,

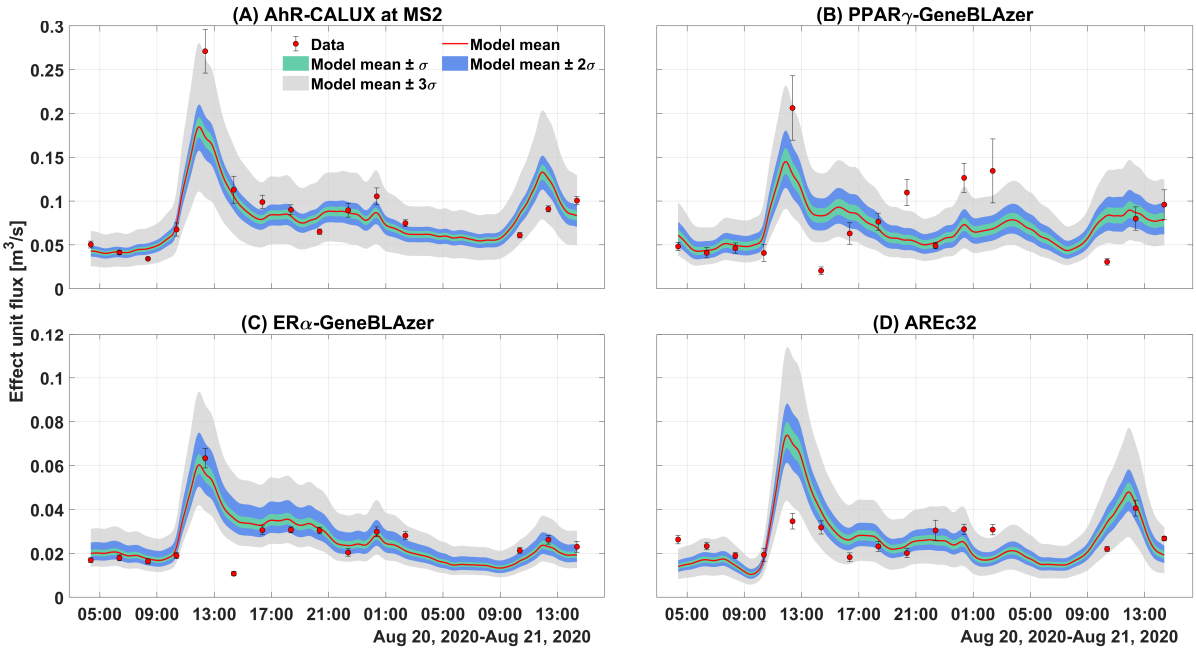

Figure 4: EU_{bio} fluxes ensemble at MS2

pronounced flux peaks were seen at around 12:00 on August 20. However, the individual temporal pattern in each bioassay could also be differentiated. In both PPARγ and ERα (Figure 4B – C), a pronounced drop of EU_{bio} flux could be observed at around 15:00. At the same time, the mean TU_{bio} flux also experienced the drop (Figure S61), indicating that the observation could not have been caused by masking effect by the cytotoxicity. Furthermore, in comparison with the other three bioassays, the measured EU_{bio} fluxes in AREc32 (Figure 4D) could clearly be seen experiencing smaller temporal oscillations. The convolution-based reactive transport model coupled with the MH-MCMC yielded the EU_{bio} fluxes ensemble after all chains converged, and the statistics of the modeled effect fluxes ensemble were computed. Depicted in Figure 4, the means and three interval estimates (one to three standard deviations) of the modeled EU_{bio} fluxes ensemble were demonstrating very good coverage of the observations. Most of the observations fell within certain envelopes of the modeled ensemble results. Moreover, the main features of the fluxes peaks in all bioassays were clearly reproduced by the model. Particularly in the case of ERα, 11 out of the 15 measurements (including the corresponding standard errors) fell within the range of one standard deviation of the mean of the model ensemble, and the observation at around 14:00 on August 20th was within the range of two standard deviations of the ensemble mean. The poorest model fit was in the case of PPARγ (Figure 4B) where only six out of the 15 data points were inside the range of one standard deviation of the mean of the model ensemble. However, as previously discussed, the largest measurement standard errors were found in the data set in PPARγ, and as a consequence the low likelihood values during the parameter searching process by the Markov chains were produced, which was further substantiated in Figure S64 that PPARγ needed the largest number of iterations for all five Markov chains to converge. The ensemble of EU_{bio} in the four bioassays at MS3 are displayed in Figure S58.

In the case of the toxic unit of the whole bioactive mixture (TU_{bio}), the measured TU_{bio} values in different bioassays should be relatively similar, since TUs are quantified based on the same endpoint, even in different bioassays. The model coupled with MH-MCMC was

only applied to the mean TU_{bio} (Section 2) measured in AhR, PPARγ, ERα and AREc32. The modeled time course ensemble of TU_{bio} at MS2 and MS3 are plotted in Figure S59 – Figure S60, respectively. Figure S61 – Figure S62 depict the modeled TU_{bio} flux ensembles. Similar to EU_{bio} flux, the modeled TU_{bio} flux ensemble were able to reproduce the flux peak in the data at both MS2 and MS3. At MS2, six out of the 15 the observations are in the range of one standard deviation of the mean ensemble, considering the measurement uncertainties. Five more are in the range of one standard deviation of the mean ensemble. At MS3, all observations are covered within the ensemble. The number of iterations the MH-MCMC took to converge for each bioassay data are given in Figure S63 - Figure S70.

4.3 Sources of micropollutants

To identify the source(s) of the micropollutants, grab samples were taken at MS up and measuring station Ehrenbach (MS Ehr), the measuring station at the WWTP effluent, measuring station Mühlbach (MS Muehl) and MS1 (sampling map: Figure S1). The concentrations of all compounds in grab samples are given in Table S3 and illustrated in Figure S73. As expected the typical WWTP effluent substances were not detected at MS up and MS Ehr, but could be found at MS Muehl and MS1. Still, atrazine-2-hydroxy, mecoprop, terbuthylazine-2-hydroxy and carbendazim were found at MS up and MS Ehr. Additionally, atrazine, atrazine-desethyl, nicosulfuron, terbuthylazine and tebuconazole were also detected at MS Ehr (Table S3). All of these compounds are either herbicides (herbicides metabolites) or fungicides (Table S1) that could come from other sources, e.g. agricultural fields during their application periods.[35]

Figure 5 depicts the grab samples' EU of individual detected compounds (EU_{chem_i}), the mixture of all detected compounds (EU_{chem}) and the total mixture (EU_{bio}) quantified in PPARγ. Results from bioassays AhR and AREc32 are shown in Figure S74. At all sampling locations, 15 out of the 42 contaminants found in the grab samples showed at least one specific effect (EC10 values of individual compounds are in Table S5). Diuron,

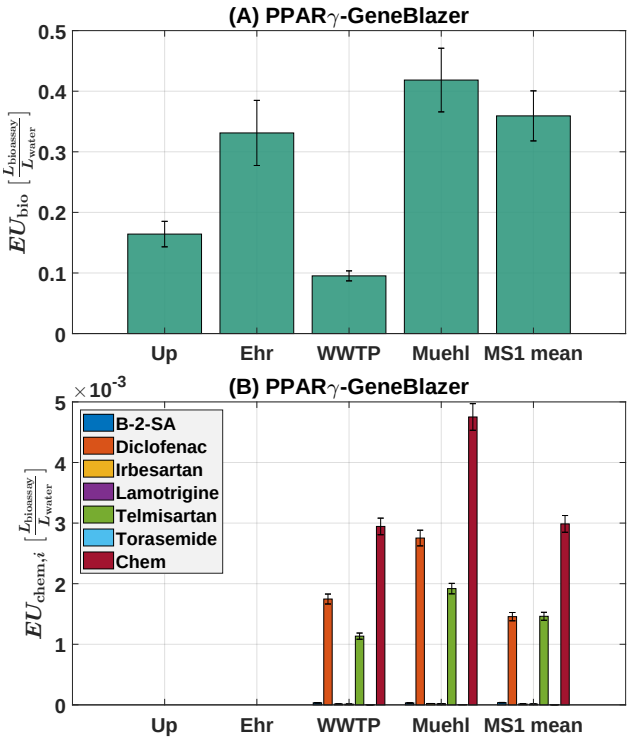

Figure 5: The effect units (EU) of grab samples: (A) Total mixture effect (EU_{bio}); (B) Individual effects $EU_{\text{chem},i}$; No grab samples were taken at MS2 and MS3. Measurement uncertainties (standard deviation) are shown by the error bars. Abbreviations: Ehr – Ehrenbach; Muehl – Mühlbach; B-2-SA – Benzothiazole-2-sulfonic acid; Chem – Effect units of the sum of detected bioactive compounds (Eq. 3).

isoproturon, and tramadol were active in two of the three bioassays. 2-aminobenzothiazole and benzothiazole-2-sulfonic acid triggered specific effects in all three bioassays. At MS Up and MS Ehr, none of the detected compounds displayed any specific effects, indicating that at those two locations, the detected chemicals made no contributions to the EU_{bio}, in terms of triggering the modes of action quantified by AhR, PPARγ and AREc32. None of the target analytes activated ERα. EU_{bio} of grab samples in ERα is shown in Figure S75. At the same locations (MS Up and MS Ehr), the EU_{bio} from grab samples were also less than 0.01 (inverse of 100 REF) in AhR, ERα and AREc32, but activated effects in PPARγ. Similar results can be found when looking at cytotoxicity. TU_{bio} of grab samples were quantified and above the limit of detection in AhR, PPARγ, ERα and AREc32 (Figure S76 – Figure S78). The total bioactive mixture from MS Up and MS Ehr showed cytotoxicity in all four bioassays.

EU_{bio} and TU_{bio} were measured at unexpectedly high values at locations upstream from the WWTP. In PPARγ, EU_{bio} from MS Up and MS Ehr were both higher than that from the WWTP effluent. In AhR and PPARγ, TU_{bio} from MS UP and MS Ehr were both higher than that in samples from WWTP effluent (Figure S76). Oddly, in AREc32 and ERα, the TU_{bio} of the WWTP effluent was less than 0.01. Still, in AREc32 and ERα, TU_{bio} of MS Up and MS Ehr were measured at the same order of magnitude to that of measuring station Mühlbach (MS Mühl) and MS1.

The results suggest that micropollutants from MS Up and MS Ehr can not activate the modes of action of aryl hydrocarbon receptor induction, estrogenicity and oxidative stress response. But even without the input from the WWTP, there are unknown chemicals in the river that are potent enough to activate the peroxisome proliferator–activated receptor activity, as well as to show cytotoxicity in AhR, PPARγ, ERα and AREc32. The presence of unknown compounds triggering specific effect in PPARγ, as well as showing strong cytotoxicity in all four bioassays, might be attributed to undetected biocides or pesticides diffusion. Previous study[35] pointed out that biocides and pesticides can migrate from mixed lands and urban areas into rivers via routes caused by rain events (e.g. disperse losses and combined sewer overflows). Existing natural compounds in rivers may also activate effects in bioassays. Salam et al.[36] and Rau et al.[37] confirmed that strong PPARγ agonists can be from plants and herbs (e.g., psi-baptigenin and hesperidin), which were not on our list of target analytes (Table S1). Further discussion on $TU_{\text{chem},i}$ of grab samples can be found in the Supporting Information (Text S24).

From individual micropollutants to the total mixture: prior and posterior distribution of the reaction constants The $EU_{\text{chem},i}$ observations from the individual micropollutants were illustrated together with EU_{bio} across all MSs in the main channel in Figure S79. Echoing grab samples shown in Figure 5, $EU_{\text{chem},i}$ at all three MSs were out-weighted by EU_{bio}. Corroboratory results were reported from numerous previous stud-

ies.[6,14,26,33,38] The potentially large number of none-detected micropollutants in the mixture were considered the main contributors to the total specific mixture effects.

Only limited numbers of micropollutants in the mixture could be identified, of which the reaction constants could be quantified. Within Bayesian inference, the reaction constants of the effects of the total mixture (EU_{bio} and TU_{bio}) were treated as random variables. The posterior distributions of the random variables were quantified (1) based on previous knowledge of individual micropollutants that were possibly in the mixture (the prior), and (2) conditioning on the data (the likelihood). Prior and posterior distributions of reaction constants for EU_{bio} and mean TU_{bio} are in Figure S63 – Figure S72.

4.4 Outlook

There is a lack of mechanistic models applied to mixture effects in rivers. We demonstrated that the in-stream processes of the mixture effects can be described by the 1D advection-dispersion-reaction equation. The computationally cheap convolution-based reactive transport model can be applied not only to simulate the effects of a large number of individual compounds detected in the mixture, but also to be coupled with stochastic methods to provide quantitative insights of the fate of the overall mixture effects.

Different transfer functions can be tested so that more insights about the process of the mixture effects in different systems (e.g. on suspended particles) can be provided. Time dependent parameters can also included, for instance, when modeling transient source(s) from tributaries during rain events, even in the stochastic processes (e.g. hierarchical model). A next step should be to test if this approach can also be applied to the micropollutant mixture effects during storm events, including the micropollutant effects associated with river sediments.

Associated content

Supporting information

The supporting information is available free of charge at `https://pubs.acs.org/doi....`

Additional information on field campaign, electrical conductivity signal correction, discharge calculation, chemical analysis, bioassays, modeled concentration, modeled mass fluxes, modeled EU and TU results (pdf). Excel file contains EC10 and IC10 values of all bioactive compounds, measured chemical concentration data, measured EU and TU data from grab samples and time series samples.

Author information

Corresponding Author

Christiane Zarfl – *Center for Applied Geoscience, Eberhard Karls University of Tübingen, Tübingen, Germany;* Email: `christiane.zarfl@uni-tuebingen.de`; Phone: + (49) 7071/29 - 76076; Fax: +(49) 7071 / 29 - 5059

Authors

Ran Wei – *Center for Applied Geoscience, Eberhard Karls University of Tübingen, Tübingen, Germany*

Beate I. Escher – *Center for Applied Geoscience, Eberhard Karls University of Tübingen, Tübingen, Germany; Department of Cell Toxicology, UFZ-Helmholtz Centre for Environmental Research, Leipzig, Germany*

Clarissa Glaser – *Center for Applied Geoscience, Eberhard Karls University of Tübingen, Tübingen, Germany*

Maria König – *Department of Cell Toxicology, UFZ-Helmholtz Centre for Environmental Research, Leipzig, Germany*

Rita Schlichting – *Department of Cell Toxicology, UFZ-Helmholtz Centre for Environ-*

mental Research, Leipzig, Germany

Markus Schmitt – *Center for Applied Geoscience, Eberhard Karls University of Tübingen, Tübingen, Germany*

Anna Störiko – *Center for Applied Geoscience, Eberhard Karls University of Tübingen, Tübingen, Germany*

Michelle Viswanathan – *Institute of Soil Science and Land Evaluation, University of Hohenheim, Hohenheim, Germany*

Author contributions

Conceptualization, R.W., C.Z., B.E., C.G, M.S.; Field campaign, C.G., R.W.; Chemical analysis and chemical data evaluation, M.S.; Bioassay experiment and effects data evaluation, M.K., R.S., B.E.; Modeling and modeled results evaluation, R.W., A.S., M.V.; Writing - reviewing and editing, R.W., C.Z., B.E; All authors have reviewed the manuscript.

Notes

The authors declare no competing financial interest.

Acknowledgement

The present study was funded by the German Research Foundation DGF [Collaborative Research Centre 1253 CAMPOS (Project P1: Rivers) DFG grant SFB 1253/1 2017]. R. Wei is supported by the German Research Foundation (DFG) in the framework of the Research Training Group GRK 1829 "Integrated Hydrosystem Modelling". The authors thank Marc Schwientek and Gaëlle Guillet for their help on the field experiment design; Jonas Allgeier for the technical support in MATLAB and LaTeX; James Awelia, Jenny Knab, Sina Lory, Oliver Nied, Bernice Nisch, Stephanie Nowak, Linda Roth, and Franziska Schädler for their

support of sampling and sample preparation; Victor Carvalho Cabral for creating the sampling site map. We gratefully acknowledge access to the platform CITEPro (Chemicals in the Environment Profiler) funded by the Helmholtz Association for bioassay measurements.

References

(1) Petrovic, M.; De Alda, M. J. L.; Diaz-Cruz, S.; Postigo, C.; Radjenovic, J.; Gros, M.; Barcelo, D. Fate and removal of pharmaceuticals and illicit drugs in conventional and membrane bioreactor wastewater treatment plants and by riverbank filtration. *Philos. Trans. R. Soc. A Math. Phys. Eng. Sci.* **2009**, *367*, 3979–4003.

(2) Kim, M.-K.; Zoh, K.-D. Occurrence and removals of micropollutants in water environment. *Environ. Eng. Res.* **2016**, *21*, 319–332.

(3) Radjenović, J.; Petrović, M.; Barceló, D. Fate and distribution of pharmaceuticals in wastewater and sewage sludge of the conventional activated sludge (CAS) and advanced membrane bioreactor (MBR) treatment. *Water Res.* **2009**, *43*, 831–841.

(4) Guillossou, R.; Le Roux, J.; Mailler, R.; Vulliet, E.; Morlay, C.; Nauleau, F.; Gasperi, J.; Rocher, V. Organic micropollutants in a large wastewater treatment plant: What are the benefits of an advanced treatment by activated carbon adsorption in comparison to conventional treatment? *Chemosphere* **2019**, *218*, 1050–1060.

(5) Mandaric, L.; Mor, J. R.; Sabater, S.; Petrovic, M. Impact of urban chemical pollution on water quality in small, rural and effluent-dominated Mediterranean streams and rivers. *Sci. Total Environ.* **2018**, *613-614*, 763–772.

(6) Neale, P. A. et al. Development of a bioanalytical test battery for water quality monitoring: Fingerprinting identified micropollutants and their contribution to effects in surface water. *Water Res.* **2017**, *123*, 734–750.

(7) Li, Z.; Sobek, A.; Radke, M. Fate of Pharmaceuticals and Their Transformation Products in Four Small European Rivers Receiving Treated Wastewater. *Environ. Sci. Technol.* **2016**, *50*, 5614–5621.

(8) Jaeger, A.; Posselt, M.; Betterle, A.; Schaper, J.; Mechelke, J.; Coll, C.; Lewandowski, J. Spatial and temporal variability in attenuation of polar organic micropollutants in an urban lowland stream. *Environ. Sci. Technol.* **2018**, *53*, 2383–2395.

(9) Schaper, J. L.; Posselt, M.; Bouchez, C.; Jaeger, A.; Nuetzmann, G.; Putschew, A.; Singer, G.; Lewandowski, J. Fate of Trace Organic Compounds in the Hyporheic Zone: Influence of Retardation, the Benthic Biolayer, and Organic Carbon. *Environ. Sci. Technol.* **2019**, *53*, 4224–4234.

(10) Müller, M. E.; Werneburg, M.; Glaser, C.; Schwientek, M.; Zarfl, C.; Escher, B. I.; Zwiener, C. Influence of Emission Sources and Tributaries on the Spatial and Temporal Patterns of Micropollutant Mixtures and Associated Effects in a Small River. *Environ. Toxicol. Chem.* **2020**, *39*, 1382–1391.

(11) Schwientek, M.; Guillet, G.; Rügner, H.; Kuch, B.; Grathwohl, P. A high-precision sampling scheme to assess persistence and transport characteristics of micropollutants in rivers. *Sci. Total Environ.* **2016**, *540*, 444–454.

(12) Glaser, C.; Zarfl, C.; Werneburg, M.; Böckmann, M.; Zwiener, C.; Schwientek, M. Temporal and spatial variable in-stream attenuation of selected pharmaceuticals. *Sci. Total Environ.* **2020**, *741*, 1–11.

(13) Guillet, G.; Knapp, J. L. A.; Merel, S.; Cirpka, O. A.; Grathwohl, P.; Zwiener, C.; Schwientek, M. Fate of wastewater contaminants in rivers: Using conservative-tracer based transfer functions to assess reactive transport. *Sci. Total Environ.* **2019**, *656*, 1250–1260.

(14) Neale, P. A.; Ait-Aissa, S.; Brack, W.; Creusot, N.; Denison, M. S.; Deutschmann, B.; Hilscherová, K.; Hollert, H.; Krauss, M.; Novák, J.; Schulze, T.; Seiler, T. B.; Serra, H.; Shao, Y.; Escher, B. I. Linking in Vitro Effects and Detected Organic Micropollutants in Surface Water Using Mixture-Toxicity Modeling. *Environ. Sci. Technol.* **2015**, *49*, 14614–14624.

(15) Neale, P. A.; Munz, N. A.; Ait-Aissa, S.; Altenburger, R.; Brion, F.; Busch, W.; Escher, B. I.; Hilscherová, K.; Kienle, C.; Novák, J.; Seiler, T. B.; Shao, Y.; Stamm, C.; Hollender, J. Integrating chemical analysis and bioanalysis to evaluate the contribution of wastewater effluent on the micropollutant burden in small streams. *Sci. Total Environ.* **2017**, *576*, 785–795.

(16) Escher, B.; Braun, G.; Zarfl, C. Exploring the Concepts of Concentration Addition and Independent Action Using a Linear Low-Effect Mixture Model. *Environ. Toxicol. Chem.* **2020**, *39*, 2552–2559.

(17) Müller, M. E.; Escher, B. I.; Schwientek, M.; Werneburg, M.; Zarfl, C.; Zwiener, C. Combining in vitro reporter gene bioassays with chemical analysis to assess changes in the water quality along the Ammer River, Southwestern Germany. *Environ. Sci. Eur.* **2018**, *30*, 5–8.

(18) Liu, Y.; Zarfl, C.; Basu, N. B.; Cirpka, O. A. Modeling the Fate of Pharmaceuticals in a Fourth-Order River Under Competing Assumptions of Transient Storage. *Water Resour. Res.* **2020**, *56*.

(19) Escher, B. I.; Neale, P. A.; Leusch, F. D. *Bioanalytical Tools in Water Quality Assessment*; IWA Publishing, 2021.

(20) Escher, B. I.; Neale, P. A. Effect-Based Trigger Values for Mixtures of Chemicals in Surface Water Detected with In Vitro Bioassays. *Environ. Toxicol. Chem.* **2021**, *40*, 487–499.

(21) Maloszewski, P.; Zuber, A. Principles and practice of calibration and validation of mathematical models for the interpretation of environmental tracer data in aquifers. *Adv. Water Resour.* **1993**, *16*, 173–190.

(22) Maloszewski, P.; Zuber, A. *Lumped Parameter Models for the Interpretation of Environmental Tracer Data (IAEA-TECDOC–910)*; 1996; pp 9–58.

(23) Glaser, C.; Zarfl, C.; Rügner, H.; Lewis, A.; Schwientek, M. Analyzing particle-associated pollutant transport to identify in-stream sediment processes during a high flow event. *Water* **2020**, *12*.

(24) Schmitt, M.; Wack, K.; Glaser, C.; Wei, R.; Zwiener, C. Separation of Photochemical and Non-Photochemical Diurnal In-Stream Attenuation of Micropollutants. *Environ. Sci. Technol.* **2021**, *55*, 8908–8917.

(25) Escher, B. I.; Neale, P. A.; Villeneuve, D. L. The advantages of linear concentration–response curves for in vitro bioassays with environmental samples. *Environ. Toxicol. Chem.* **2018**, *37*, 2273–2280.

(26) König, M.; Escher, B. I.; Neale, P. A.; Krauss, M.; Hilscherová, K.; Novák, J.; Teodorović, I.; Schulze, T.; Seidensticker, S.; Kamal Hashmi, M. A.; Ahlheim, J.; Brack, W. Impact of untreated wastewater on a major European river evaluated with a combination of in vitro bioassays and chemical analysis. *Environ. Pollut.* **2017**, *220*, 1220–1230.

(27) van Ravenzwaaij, D.; Cassey, P.; Brown, S. D. A simple introduction to Markov Chain Monte–Carlo sampling. *Psychon. Bull. Rev.* **2018**, *25*, 143–154.

(28) Gelman, A.; Carlin, J. B.; Stern, H. S.; Dunson, D. B.; Vehtari, A.; Rubin, D. B. *Bayesian Data Analysis*, 3rd ed.; 2021.

(29) Mansouri, K.; Grulke, C. M.; Judson, R. S.; Williams, A. J. OPERA models for pre-

dicting physicochemical properties and environmental fate endpoints. *J. Cheminform.* **2018**, *10*, 1–19.

(30) Brooks, S. P.; Gelman, A. General methods for monitoring convergence of iterative simulations. *J. Comput. Graph. Stat.* **1998**, *7*, 434–455.

(31) Gelman, A.; Rubin, D. B. Inference from Iterative Simulation Using Multiple Sequences. *Stat. Sci.* **1992**, *7*, 457–472.

(32) Kloepfer, A.; Jekel, M.; Reemtsma, T. Occurrence, sources, and fate of benzothiazoles in municipal wastewater treatment plants. *Environ. Sci. Technol.* **2005**, *39*, 3792–3798.

(33) Neale, P. A. et al. Assessing the Mixture Effects in in Vitro Bioassays of Chemicals Occurring in Small Agricultural Streams during Rain Events. *Environ. Sci. Technol.* **2020**, *54*, 8280–8290.

(34) Müller, M. E.; Zwiener, C.; Escher, B. I. Storm Event–Driven Occurrence and Transport of Dissolved and Sorbed Organic Micropollutants and Associated Effects in the Ammer River, Southwestern Germany. *Environ. Toxicol. Chem.* **2021**, *40*, 88–99.

(35) Wittmer, I. K.; Bader, H. P.; Scheidegger, R.; Singer, H.; Lück, A.; Hanke, I.; Carlsson, C.; Stamm, C. Significance of urban and agricultural land use for biocide and pesticide dynamics in surface waters. *Water Res.* **2010**, *44*, 2850–2862.

(36) Salam, N. K.; Huang, T. H.; Kota, B. P.; Kim, M. S.; Li, Y.; Hibbs, D. E. Novel PPAR-gamma agonists identified from a natural product library: A virtual screening, induced-fit docking and biological assay study. *Chem. Biol. Drug Des.* **2008**, *71*, 57–70.

(37) Rau, O.; Wurglics, M.; Dingermann, T.; Abdel-Tawab, M.; Schubert-Zsilavecz, M. Screening of herbal extracts for activation of the human peroxisome proliferator-activated receptor. *Pharmazie* **2006**, *61*, 952–956.

(38) Escher, B. I.; Neale, P. A.; Leusch, F. D. L. Effect-based trigger values for invitro bioassays: Reading across from existing water quality guideline values. *Water Res.* **2015**, *81*, 137–148.

TOC Graphic

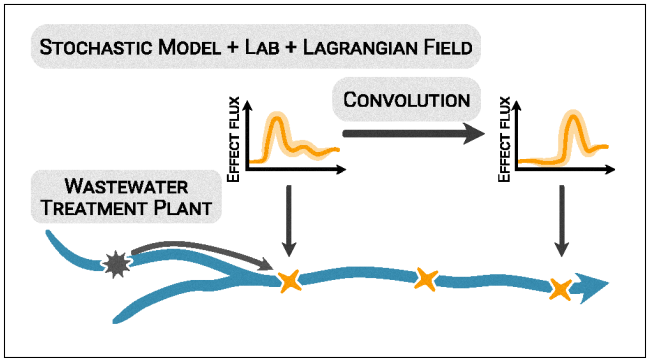
STOCHASTIC MODEL + LAB + LAGRANGIAN FIELD
CONVOLUTION
EFFECT FLUX
EFFECT FLUX
WASTEWATER TREATMENT PLANT